EFFECTS OF NONLINEAR ENERGY SINK ON THE AEROELASTIC BEHAVIOR OF AN ELECTROMECHANICALLY COUPLED TYPICAL SECTION

Gabriela Mayumi de Freitas Otsubo, Tarcisio Marinelli Pereira Silva, Douglas D'Assunção, Carlos De Marqui Jr.
Department of Aeronautical Engineering, Sao Carlos School of Engineering, University of Sao Paulo, Sao Carlos, Sao Paulo, Brazil
Keywords: *Nonlinear Energy Sink, Aeroelastic Control, Piezoelectricity*

Abstract

Several researches have investigated the use of essentially nonlinear attachments, such as a nonlinear energy sink (NES), coupled to a linear host structure. NES devices efficiently reduce vibrations due to the one-way energy flow from the host structure to the nonlinear attachment, where it is localized and dissipated. NES devices also do not possess any preferential resonance frequency, enabling frequency-wise wideband performance and robustness against detuning. In this work, the interactions between an essentially nonlinear piezoelectric attachment and an electromechanically coupled two-degree-of-freedom (2-DOF) aeroelastic typical section are investigated. Equations of motion are derived to model the 2-DOF typical section with piezoelectric coupling added to the plunge DOF. An equivalent electrical circuit of the piezoaeroelastic system is presented and employed in the simulations of the system in short-circuit condition and also combined to the NES.

1 Introduction

Piezoelectric materials have been employed for passive vibration control. In such case, the terminals of the piezoelectric material are combined to a passive circuit where energy is dissipated. The first piezoelectric shunt damping circuits investigated in the literature were the resistive [1], the inductive [2], and resistive-inductive ones [3,4]. The effect of a resistive shunt is analogous to the constrained-layer damping technique [5]. The inductive shunt allows the cancelation of the impedance of the piezoelectric capacitance, increasing the energy flow between mechanical and electrical domain. Knowing from Uchino and Ishii [1] that a resistor creates a damping effect, Hagood and von Flotow [3] and Wu [4] studied the effect of a resistor connected to an inductor and realized the damped dynamic vibration absorber effect. Different piezoelectric shunt damping techniques have been widely investigated in the literature as reported in review articles by Lesieutre [5] and Ahmadian and Deguilio [6].

The resistive-inductive (RL) shunts are effective in the neighborhood of a target frequency. Any frequency mistuning (due to design uncertainties, ageing and external conditions) results in reduced performance to attenuate vibrations. Moreover, low target frequencies require very high and unpractical inductances.

Researchers have explored nonlinear piezoelectric shunt circuits in order to enable broader frequency bandwidth performance. Agnes and Inman [7] investigated a nonlinear piezoelectric absorber and reported a weak performance on vibration attenuation. More recently, Soltani and Kerschen [8] explored the effects of a nonlinear piezoelectric tuned vibration absorber designed to attenuate vibrations of a nonlinear primary system.

Researchers have also investigated essentially nonlinear mechanical attachment in

order to enable NES [9]. Gendelman and his co-authors [9-11] were the first to report the nonlinear energy-pumping phenomenon (or targeted energy transfer) that can be observed in NES. It is characterized by the irreversible energy transfer from the primary system to the vibration absorber, where energy is localized and dissipated due to the presence of a damper. The effects of mechanical NES (essentially nonlinear mass-spring systems) on the behavior of aeroelastic systems have already been reported in the literature. Lee et al. [12] investigated the effects of a mechanical NES device connected to a nonlinear typical section and the numerical results were validated against experimental data from wind tunnel tests. The effects of a rotational NES on the aeroelastic behavior of a flexible wind have also been reported [13-15].

While many researchers reported in the literature investigates mechanical approaches for a NES device only a few have discussed a piezoelectric based NES. Zhou et al. [16] report the use of piezoelectric based NES on mistuned bladed disks. The sink is obtained by associating piezoelectric material an electrical circuit composed by an RL circuit in series with a negative capacitance and a nonlinear capacitance. The nonlinear capacitance provides a cubic voltage to charge relation required for the NES, while the negative capacitance is employed to reduce the internal capacitance of the piezoelectric material.

In this paper, we investigate the effects of a piezoelectric NES on the aeroelastic behavior of an electromechanically coupled 2-DOF typical section. The electromechanical coupling is added to the plunge DOF. An electrical circuit based on the approach presented by Zhou et al. [16] is presented to obtain the piezoelectric based NES. The equations of motion of the typical section and also an unsteady aerodynamic model are presented. An equivalent electrical circuit is derived to represent the piezoaereoelastic typical section in electrical domain and also to include the nonlinear shunt circuit in the solution. Numerical results show that the piezoelectric NES device yields a substantial increase of the flutter envelope of the typical section, assuming the short-circuit condition as the baseline.

2 Aeroelastic Typical Section

Figure 1 displays the 2-DOF typical section. The plunge and pitch displacements are denoted by h and α, respectively. In addition, b is the semichord length, U is the airflow speed, $x_\alpha b$ is the distance of the axis of rotation from the center of gravity, K_h and K_α are the stiffness per unit length for plunge and pitch, B_h and B_α are the damping coefficient per unit length for plunge and pitch, M is the aerodynamic moment per length and F is the aerodynamic lift per length.

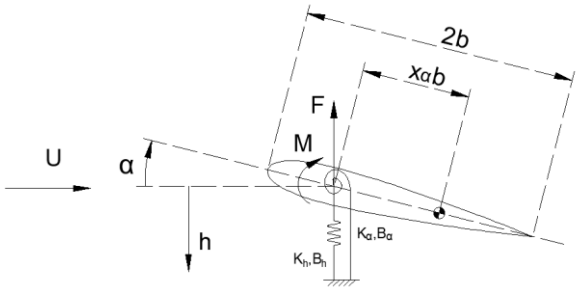

Fig. 1. Typical Section Model

Adding piezoelectric coupling to the plunge DOF of the typical section, the equations of the electromechanically coupled system are

$$\left(m+m_f\right)\ddot{h}+mx_\alpha b\ddot{\alpha}+B_h\dot{h}+ \quad (1)$$
$$+K_h h-\frac{\theta V_p}{l}=-F$$

$$mx_\alpha b\ddot{h}+I_\alpha\ddot{\alpha}+B_\alpha\dot{\alpha}+K_\alpha\alpha=M \quad (2)$$

$$C_p V_p+q+\theta h=0 \quad (3)$$

where l is the span length, m is the airfoil mass per unit length, m_f is the fixture mass per unit length (connecting the airfoil to the plunge springs), I_α is the moment of inertia per unit length about the elastic axis, Cp is the inherent capacitance of the piezoelectric material, V_p is the voltage across the shunted circuit, θ is the electromechanical coupling and q is the electrical charge.

Using Theodorsen's unsteady thin airfoil theory [17], the aerodynamic loads are calculated as

$$F = \rho U^2 F_h h + \rho U b F_{\dot{h}} \dot{h} + \\ + \rho U^2 b F_\alpha \alpha + \rho U b^2 F_{\dot{\alpha}} \dot{\alpha} \quad (4)$$

$$M = \rho U^2 M_h h + \rho U b^2 M_{\dot{h}} \dot{h} + \\ + \rho U^2 b^2 M_\alpha \alpha + \rho U b^3 M_{\dot{\alpha}} \dot{\alpha} \quad (5)$$

where F_h, $F_{\dot{h}}$, F_α, $F_{\dot{\alpha}}$, M_h, $M_{\dot{h}}$, M_α, $M_{\dot{\alpha}}$ are oscillatory aerodynamic derivatives and ρ is the air density. Assuming harmonic condition in equations (6) and (7) and substituting in equations (1) and (2) results

$$L_h \ddot{h} + R_h \dot{h} + \frac{1}{C_h} h + m x_\alpha b \ddot{\alpha} + \\ + e_2 \dot{\alpha} + e_3 \alpha - \frac{\theta}{l} V_p = 0 \quad (6)$$

$$L_\alpha \ddot{\alpha} + R_\alpha \dot{\alpha} + \frac{1}{C_\alpha} \alpha + \\ + m x_\alpha b \ddot{h} + e_5 \dot{h} + e_6 h = 0 \quad (7)$$

where e_n represent the remaining aerodynamic terms.

An equivalent electrical circuit of the electromechanically coupled typical section can be obtained [18]. In such case, the inertia, stiffness and damping terms of equations (1) and (2) are replaced by its electrical analogs: inductance (L), resistance (R) and capacitance (C), respectively. It can be noted that all terms of equations (6) and (7) are proportional to structural displacement and velocity. In the equivalent circuit, each equation is represented by an RLC circuit with voltage-controlled voltage sources, which couples both DOFs. The electromechanical coupling is represented by a voltage-controlled voltage source ($V(v_p)$) in the plunge circuit and by a current-controlled current source ($i_p(\dot{h})$) connected in parallel with the capacitor C_p in order to represent the piezoelectric material. The equivalent electrical circuit is shown in Fig. 2.

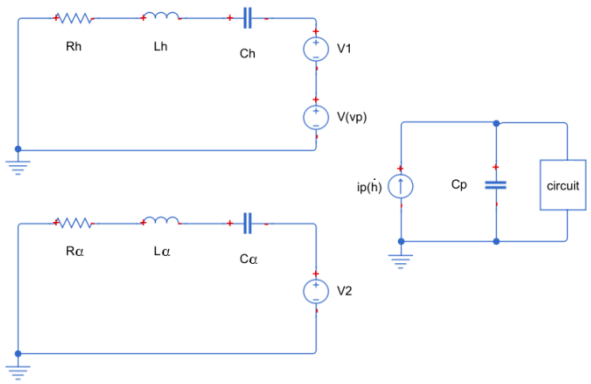

Fig. 2. Equivalent Electrical Circuit (adapted from [18])

The "circuit" block of Fig. 2 can represent different external circuits. In this paper, a piezoelectric based NES is considered which is obtained by connecting a RL circuit in series with a nonlinear capacitance and a negative capacitance, as shown in Fig. 3.

Fig. 3. Nonlinear Shunt Circuit

The negative capacitance minimizes the linear effect of the internal capacitance of piezoelectric material, which is required for a NES. The electrical equation of the NES is

$$L\ddot{q} + R\dot{q} + \frac{q}{C_{res}} + \beta q^3 + \frac{\theta}{C_p} h = 0 \quad (8)$$

where β is the nonlinear capacitance coefficient and Cres is the residual capacitance that is related to the piezoelectric internal capacitance and negative capacitance added to the system. 3 Piezoelectric

3 Based NES Circuit

In practice, C_{neg} and C_{nl} in Figure 3 are obtained synthetically, as shown in the piezoelectric NES circuit of Fig. 4, which is included in the "circuit" block of Fig. 2 for numerical simulations.

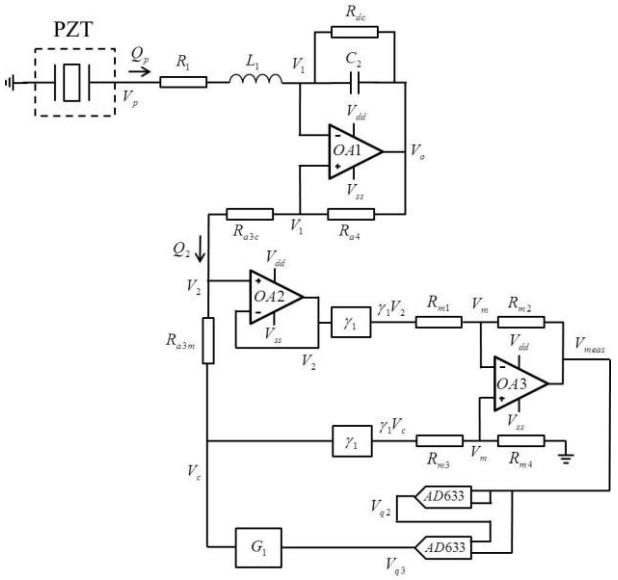

Fig. 4. Piezoelectric Nonlinear Shunt Circuit Used In Numerical Simulations

In Fig. 4, R_1 and L_1 stand, respectively, for the resistor and inductor of the piezoelectric NES. The negative capacitance is composed by the resistors R_{dc}, R_{a3c}, R_{a3m} and R_{a4}, the operational amplifier $OA1$, and the capacitor C_2. The resistor R_{dc} is used to remove any DC component in the negative capacitance circuit. The value of C_{neg} can be expressed as,

$$C_{neg} = -\frac{R_{a4}C_2}{R_{a3c}+R_{a3m}} \tag{9}$$

The cubic nonlinear capacitor is obtained through the voltage term $V_c = \beta q^3$. The voltage V_c is obtained through the operational amplifiers $OA2$ and $OA3$, the resistors R_{m1} to R_{m4}, the two voltage multipliers AD633 and the voltage gains γ_1 and G_1. The gain γ_1 stands for voltage divider circuits. In case $\max(V_c) > V_{sat}$ (where V_{sat} is the saturation voltage of $OA3$), γ_1 assumes the value $V_{sat}/\max(V_c)$ to ensure $OA3$ does not saturate. In case $\max(V_c) \le V_{sat}$, γ_1 becomes equal to one. When $\gamma_1 = 1$, the voltage divider gain is not necessary and can be replaced by a short-circuit. The voltage V_c is given by,

$$V_c = G_1 G^3 \left(\frac{R_{a3m}}{R_{a4}C_2}\right)^3 \frac{q^3}{100} \tag{10}$$

and the gain G_1 is adjusted such that $V_c = \beta q^3$. Therefore,

$$G_1 = \frac{100\beta}{G^3}\left(\frac{R_{a4}C_2}{R_{a3m}}\right)^3 \tag{11}$$

and in case $G_1 \ge 1$, the circuit of **Erro! Fonte de referência não encontrada.**a should be used and if $G_1 < 1$, the circuit shown in **Erro! Fonte de referência não encontrada.**b should be employed. In both cases, the value of resistor R_{g3} can be chosen arbitrarily.

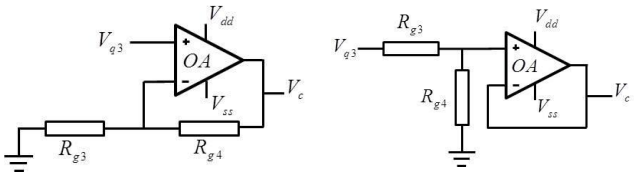

$R_{g4} = R_{g3}(G_1 - 1)$ $\qquad$ $R_{g4} = R_{g3}\dfrac{G_1}{1-G_1}$

a) b)

Fig. 5. Circuit To Provide The Voltage Gain G_1

4 Case Studies

This section presents the case studies using the equivalent electrical model of Fig. 2. In the first case, the aeroelastic behavior of the typical section with the piezoelectric material in short circuit condition is investigated, which is used as a reference. Then, in the second case, the piezoelectric based NES circuit is connected to the typical section and its aeroelastic behavior is investigated. In all simulations, an initial plunge displacement of 3 mm is assumed.

The typical section properties are shown in Table 1. Two piezoceramics (QP10n from Mide Corp.) are considered in the plunge DOF, leading to an equivalent capacitance of C_p = 120 nF and an electromechanical coupling parameter of θ = 1.55 mN/V.

Table 1. Typical section parameters

Parameter	Value

l	0.5 m
a	-0.5
b	0.125 m
$x_\alpha b$	0.0258 m
m	0.789 kg/m
m_f	1.091 kg/m
I_α	0.003 kg.m
K_α	3.13 N/rad
K_h	2193 N/m²
B_α	0.0258 N.s/rad
B_h	0.8241 N.s/rad²

4.1 Short Circuit Case

The aeroelastic behavior of a 2-DOF typical section in short-circuit condition is briefly discussed. The time responses of pitch and plunge DOFs are evaluated for different airflow speeds and the short-circuit flutter speed of the typical section is determined. Fig. 6 shows that the system is stable for airflow speeds smaller than 10.7 m/s and unstable for airflow speed larger than 10.7 m/s. Therefore, the short-circuit flutter speed is assumed as 10.7 m/s.

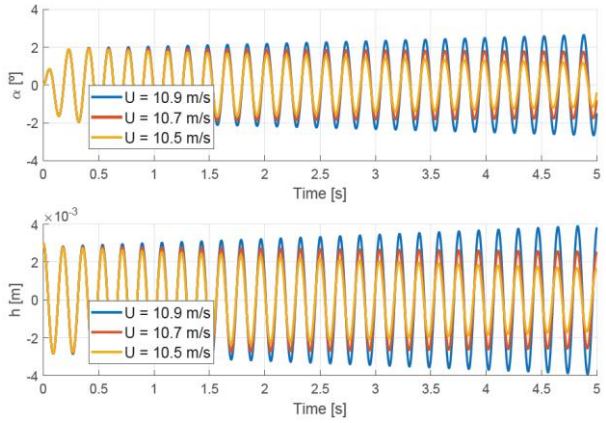

Fig. 6. Aeroelastic Behavior Of The Typical Section For The Short-Circuit Condition.

4.2 Piezoelectric NES Case

The NES parameters shown in equation (8) are obtained iteratively. Initially, the parameter C_{res} is set to eliminate the influence of the linear capacitance. Then, simulations are performed in order to determine L, R and β that yields enhanced vibration attenuation. Although eliminating the influence of the linear capacitance would be theoretically required, in practical applications, such condition leads to instabilities. Numerical simulations conducted in order to find an acceptable negative capacitance in the stable domain. The final properties of the NES are shown in Table 2.

Table 2. NES parameters

Parameter	Value
L	10 H
R	25 kΩ
β	$5x10^{14}$ V/C³
C_{res}	50 µF

Using the parameters of tables 1 and 2 in the equivalent electrical circuit simulations, the aeroelastic behavior of the typical section displayed in Figure 7 is obtained at the short-circuit flutter speed. While persistent oscillations are observed for the short-circuit condition, the use of piezoelectric based NES results in damped oscillations. The maximum voltage across the piezoceramic electrodes in Fig. 7 is 257.7 V.

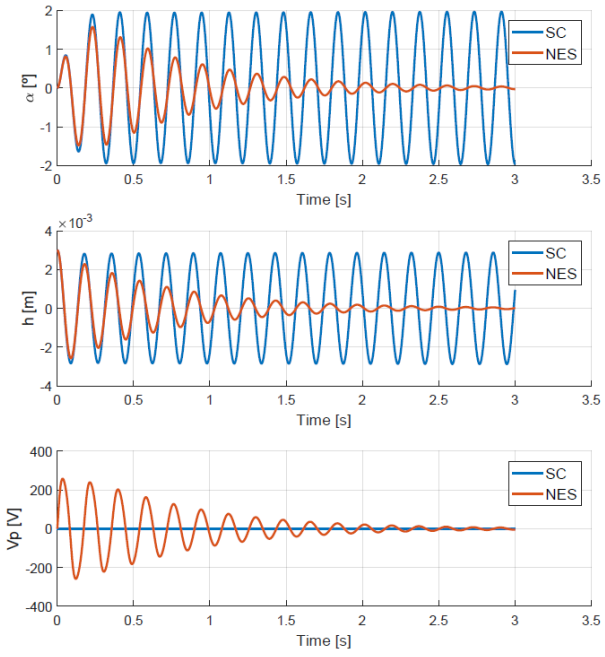

Fig. 7. Effects Of Piezoelectric NES At The Short-Circuit Flutter Speed (U = 10.76 m/s).

Fig. 8 shows aeroelastic behavior of the typical section with the piezoelectric NES for different airflow speeds above the linear short-circuit flutter speed. In such case, the system is

stable for airflow speeds smaller than 13.1 m/s, assumed as the new flutter boundary that is 22.4% larger than the short-circuit one. The maximum voltage across the piezoceramic electrodes is always smaller than 264.5 V.

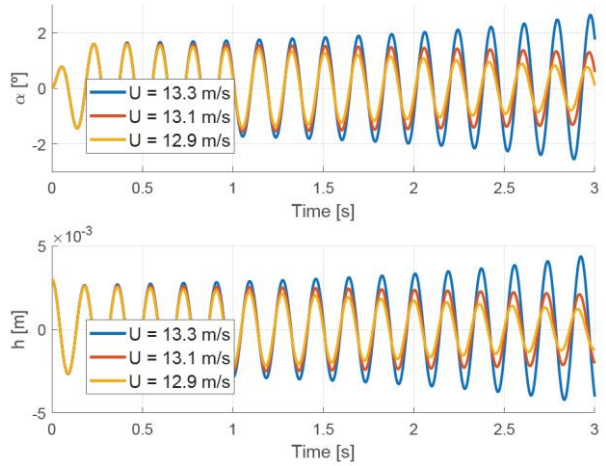

Fig. 8. Aeroelastic Behavior Of The Typical Section With The Piezoelectric NES.

Although not shown, it is important to note that the NES performance depends on the initial condition.

Fig. 9 displays the voltage-charge behavior of the linear residual capacitance, of the cubic term and also the combined one, q/C_{res} , βq^3 and $\beta q^3 + q/C_{res}$, respectively. Although a residual capacitance is present, the resulting voltage-charge is very close to a cubic one, what is enough to enable an essential nonlinear behavior.

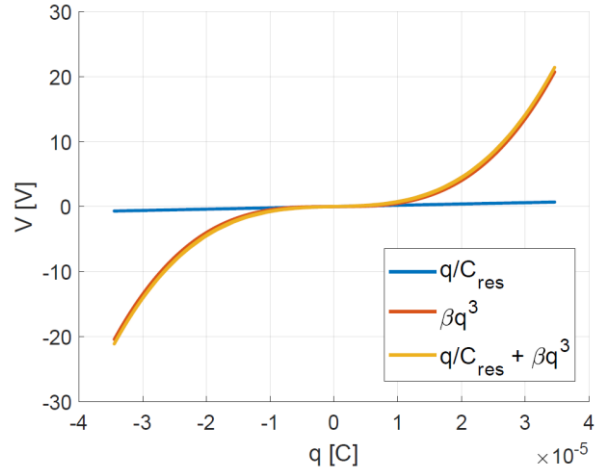

Fig. 9. Characterization Of The Nonlinear Circuit.

5 Conclusions

This paper verifies the effects of a piezoelectric based NES on the aeroelastic of a 2-DOF typical section. An equivalent electrical circuit of the typical section was presented. A NES circuit was discussed and the main electrical equations provided. The essentially nonlinear piezoelectric NES consists of a resistor, an inductor, a negative capacitance circuit and a nonlinear capacitance circuit all connected in series.

The aeroelastic behavior of the typical section in short-circuit condition was assumed as a reference case. The short-circuit flutter speed was determined as 10.7 m/s. This flutter boundary was expanded by 22.4% when the piezoelectric based NES was considered. Therefore, a piezoelectric based NES can be considered a useful method of aeroelastic control.

References

[1] Uchino K, Ishii T. Mechanical damper using piezoelectric ceramics. *J Ceram Soc Japan*. 1988;96(1116):863-867. doi:10.2109/jcersj.96.863

[2] Forward RL. Electronic damping of vibrations in optical structures. *Appl Opt*. 1979;18(5):690. doi:10.1364/AO.18.000690

[3] Hagood NW, von Flotow A. Damping of structural vibrations with piezoelectric materials and passive electrical networks. *J Sound Vib*. 1991;146(2):243-268. doi:10.1016/0022-460X(91)90762-9

[4] Wu S. Piezoeleciric shunts with a parallel R-L circuit for structural damping and vibration control. In: *Smart Structures and Materials 1996: Passive Damping and Isolation*. Vol 27201259. ; 1996:259-269. doi:10.1117/12.239093

[5] Lesieutre GA. Vibration damping and control using shunted piezoelectric materials. *Shock Vib Dig*. 1998;30(3):187-195. doi:10.1177/058310249803000301

[6] Ahmadian M, DeGuilio AP. Recent Advances in the Use of Piezoceramics for Vibration Suppression. *Shock Vib Dig*. 2001;33(1):15-22. doi:10.1177/058310240103300102

[7] Agnes GS, Inman DJ. Nonlinear piezoelectric vibration absorbers. *Smart Mater Struct*. 1996;5(5):704-714. doi:10.1088/0964-1726/5/5/018

[8] Soltani PS, Kerschen G. The nonlinear piezoelectric tuned vibration absorber. *Smart Mater Struct*. 2015;24(7). doi:10.1088/0964-1726/24/7/075015

[9] Vakakis AF, Gendelman OV, Bergman LA, McFarland DM, Kerschen G, Lee YS. *Nonlinear Targeted Energy Transfer in Mechanical and*

Structural Systems. Vol 156.; 2008. doi:10.1007/978-1-4020-9130-8

[10] Gendelman O V. Transition of energy to a nonlinear localized mode in a highly asymmetric system of two oscillators. *Nonlinear Dyn*. 2001;25(1-3):237-253. doi:10.1023/A:1012967003477

[11] Vakakis AF, Gendelman O. Energy Pumping in Nonlinear Mechanical Oscillators: Part II—Resonance Capture. *J Appl Mech*. 2001;68(1):42. doi:10.1115/1.1345525

[12] Lee YS, Vakakis AF, Bergman LA, McFarland DM, Kerschen G. Suppressing aeroelastic instability using broadband passive targeted energy transfers, part 1: theory. *AIAA J*. 2007;45(3):693-711. doi:10.2514/1.24062

[13] Hubbard SA, Fontenot RL, McFarland DM, et al. Transonic Aeroelastic Instability Suppression for a Swept Wing by Targeted Energy Transfer. *J Aircr*. 2014;51(5):1467-1482. doi:10.2514/1.C032339

[14] Hubbard SA, McFarland DM, Bergman LA, Vakakis AF. Targeted energy transfer between a model flexible wing and nonlinear energy sink. *J Aircr*. 2010;47(6):1918-1931. doi:10.2514/1.C001012

[15] Hubbard SA, McFarland DM, Bergman LA, Vakakis AF, Andersen G. Targeted Energy Transfer Between a Swept Wing and Winglet-Housed Nonlinear Energy Sink. *AIAA J*. 2014;52(12):2633-2651. doi:10.2514/1.J052538

[16] Zhou B, Thouverez F, Lenoir D. Essentially nonlinear piezoelectric shunt circuits applied to mistuned bladed disks. *J Sound Vib*. 2014;333(9):2520-2542. doi:10.1016/j.jsv.2013.12.019

[17] Theodorsen T. General theory of aerodynamic instability and the mechanism of flutter. *NACA Rep*. 1935;(No. 496):24. doi:10.1017/CBO9781107415324.004

[18] Elvin NG. Equivalent electrical circuits for advanced energy harvesting. *J Intell Mater Syst Struct*. 2014;25(14):1715-1726. doi:10.1177/1045389X14521878

6 Contact Author Email Address

mailto: gmayumio@gmail.com
mailto: tarcismarinelli@hotmail.com
mailto: douglasdassuncao@yahoo.com.br
mailto: demarqui@sc.usp.br

Copyright Statement